Physica B 480 (2016) 63–67

Contents lists available at ScienceDirect

Physica B

journal homepage: www.elsevier.com/locate/physb

# Structure, morphology and optical properties of undoped and MN-doped $ZnO_{(1-x)}S_x$ nano-powders prepared by precipitation method

F.B. Dejene [a,*], M.O. Onani [b], L.F. Koao [a], A.H. Wako [a], S.V. Motloung [a], M.T. Yihunie [a]

[a] Department of Physics, University of the Free State, (Qwa-Qwa campus), Private Bag X-13, Phuthaditjhaba 9866, South Africa
[b] Chemistry Department, University of the Western Cape, Private Bag x17, Bellville 7535, South Africa

ARTICLE INFO

*Article history:*
Received 15 May 2015
Received in revised form
21 August 2015
Accepted 24 August 2015
Available online 28 August 2015

*Keywords:*
Zinc oxide
Precipitation
Doping
Photoluminescence
Nanomaterials

ABSTRACT

The undoped and Mn-doped $ZnO_{(1-x)}S_x$ nano-powders were successfully synthesized by precipitation method without using any capping agent. Its structure, morphology, elemental analysis, optical and luminescence properties were determined by scanning electron microscopy (SEM), energy-dispersive X-ray spectroscopy (EDS), UV–vis spectroscopy (UV) and photoluminescence spectroscopy (PL). A typical SEM image of the un-doped $ZnO_{(1-x)}S_x$ nanoparticles exhibit flake like structures that changes to nearly spherical particles with Mn-doping. The XRD of undoped and Mn doped $ZnO_{(1-x)}S_x$ pattern reveals the formation of a product indexed to the hexagonal wurtzite phase of ZnS. The nanopowders have crystallite sizes estimated from XRD measurements were in the range of 10–20 nm. All the samples showed absorption maximum of $ZnO_{(1-x)}S_x$ at 271 nm and high transmittance in UV and visible region, respectively. The undoped $ZnO_{(1-x)}S_x$ nanoparticles show strong room-temperature photoluminescence with four emission bands centering at 338 nm, 384 nm, 448 nm and 705 nm that may originate to the impurity of $ZnO_{(1-x)}S_x$, existence of oxide related defects. The calculated bandgap of the nanocrystalline $ZnO_{(1-x)}S_x$ showed a blue-shift with respect to the Mn-doping. The PL spectra of the Mn-doped samples exhibit a strong orange emission at around 594 nm attributed to the $^4T_1$–$^6A_1$ transition of the $Mn^{2+}$ ions.


## 1. Introduction

Zinc sulfide (ZnS) is a versatile technologically important semiconductor material and fundamental milestone for many photonic and optoelectronic applications of quantum-con- fined species, e.g. photodetectors, light emitting diodes, lasers and biological levels [1–3]. With recent advances in colloidal chemistry, efforts have been made to synthesize high-quality semiconductor nanoparticles (NPs) in the liquid phase either by aqueous or non-aqueous route. The NPs structures are interesting from a physical and chemical point of view mainly because several of their properties are very different from those of bulk materials [4]. Especially, the significant size dependent shift in the band gap has attracted much attention. This so-called quantum-size effect allows one to tune the emission and excitation wavelengths of a nanocrystal by tuning the crystallite sizes. With a wide band gap of 3.7 eV and a large exciton binding energy of 40 meV at room temperature, which makes it an excellent candidate for exploring the intrinsic recombination processes in dense exciton systems. Moreover ZnS is also attractive for blue and ultra-violet optoelectronic devices, and transparent conducting oxide films for photovoltaic applications. The large excitonic binding energies of ZnS could enable efficient excitonic emission at temperatures well above room temperature and therefore lower threshold intensities for optoelectronic devices based on these semiconductors can be expected. Alloying ZnO by incorporating equivalent anions has not been extensively studied. Anion doping in ZnO, i.e., replacing oxygen by sulfur e.g. $ZnO_{(1-x)}S_x$ (ZnOS), has been reported recently [5,6]. Due to the large electronegativity differences between O and S it would be expected that the bowing parameters of ZnOS are large hence no linear relationship between band gap and amount of sulfur content. The change of anions in ZnO by isoelectronic impurities is important from the viewpoint of band gap engineering. Unfortunately, because of non radiative recombination of charge carriers at the surface sites that compete with band edge emission, a low photoluminescence (PL) is often observed in as prepared ZnS NPs. One of the major limitations about the formation of these materials is to control the electronic states, i.e. the exciton or the surface states, to increase the PL properties. In this

* Corresponding author.
*E-mail address:* dejenebf@qwa.ufs.ac.za (F.B. Dejene).

http://dx.doi.org/10.1016/j.physb.2015.08.043
0921-4526/

work, high-quality undoped and Mn-doped $ZnO_{(1-x)}S_x$ nanopowders were prepared by wet chemical method. In this technique, the precursor concentration, growth temperature and PH are some of the critical experimental parameters to obtain $ZnO_{(1-x)}S_x$ nanostructures of different morphologies.

## 2. Experimental details

The precipitation method was used to synthesize $ZnO_{(1-x)}S_x$ nanoparticles at room temperature. The simple and versatile technique has been found to have a number of advantages such as easy process ability at ambient conditions, possibility of doping of different kinds of impurities with high doping concentration even at room temperature, good control over the chemistry of doping and easiness of surface capping with a variety of different steps involved in the synthesis process of nanoparticles. Undoped and Mn-doped $ZnO_{(1-x)}S_x$ nanoparticles were precipitated from a mixture of zinc acetate and manganese acetate with sodium sulfide in aqueous solution. In a typical procedure, aqueous solution of sodium sulfide was added into aqueous solution of zinc acetate and aqueous solution of manganese acetate with the molar ratio of Zn:S being 1:1. The mixed solution was stirred, heated slowly and refluxed at a temperature of ~80 °C for 2 h. Then the solution was aged for few hrs to obtain white precipitate. The different concentrations of Mn taken are as follows: 0.5, 1.0, 1.5 and 12 mol%. The resulting precipitates were filtered and washed several times with distilled water and ethanol. Washings were done to remove any organic part or any other impurities from the particles. The product was dried in an oven vacuum at 100 °C for 2 h.

## 3. Results

Fig. 1(a)–(c) are scanning electron microscopy images, which show the general morphology of the product. From these images, it can be seen that the undoped $ZnO_{(1-x)}S_x$ possess mixture of irregular nanoflakes structure. The crystallites sizes are in nano range. The addition of Mn to $ZnO_{(1-x)}S_x$ changes the surface morphology to nearly spherical structures, which is characteristic of particles formed from liquid droplets. The Mn-doped $ZnO_{(1-x)}S_x$ crystallites are uniform in size. When the amount of Mn in the reaction changed from 0.5 to 1.5 mol%, the average crystallites size of the corresponding products also decreased further (Fig. 1(b) and (c)). Therefore the presence Mn ions have decreasing effect on the size of the crystallites. The decrease in average crystallites size of $ZnO_{(1-x)}S_x$ nanoparticles as the content of Mn concentration increase can be inferred from Fig. 1. An EDX spectrum taken from the same sample is shown in Fig. 2(a), and the result indicates that the nanoparticles are composed of O, Mn, Zn and S, and the approximate atomic ratios of Zn to O to S are 1:2:0.25. Quantitative analysis showed that the ZnS powders were deficient in S in terms of composition, probably due to the volatility of S. The sulfur peak seems to be more pronounce with the presence of Mn ions. A moderate carbon peak was observed in the EDX spectra due to carbon coating used on powders to overcome surface charging during measurements.

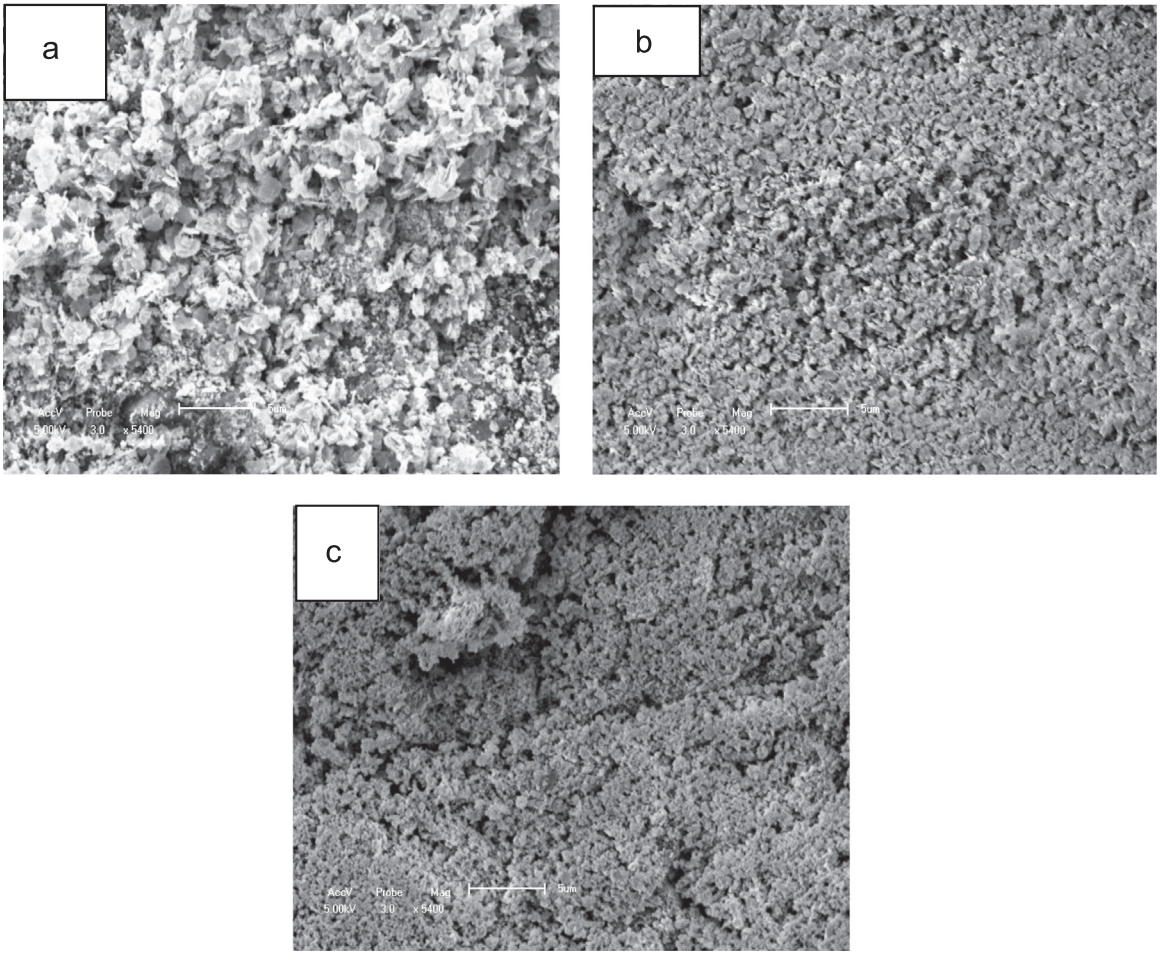


**Fig. 1.** Scanning electron micrographs of precipitation method synthesized (a) undoped, (b) 0.5 mol% and (c) 12 mol% Mn-doped $ZnO_{(1-x)}S_x$ nanoparticles.

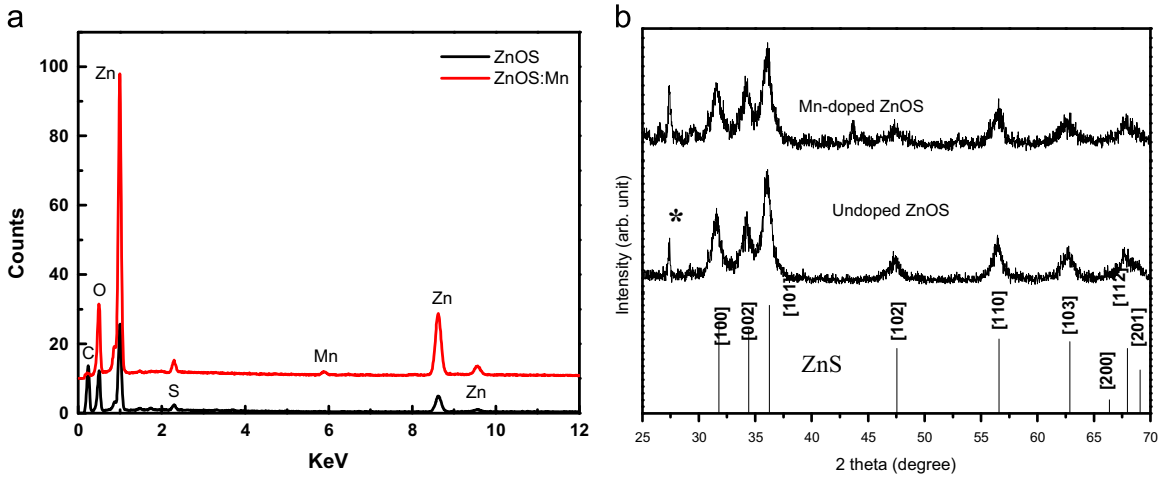


**Fig. 2.** (a) EDS spectra and (b) a representative XRD patterns of the produced undoped and Mn-doped $ZnO_{(1-x)}S_x$ nanoparticles.

A strong O peak is also observed. This may originate from the oxidation of some ZnS nanoparticles exposed to the air. The X-ray diffraction (XRD) investigation gives the information about the structure of the nanoparticles. X-ray diffraction patterns taken from undoped $ZnO_{(1-x)}S_x$, Mn doped $ZnO_{(1-x)}S_x$ (0.5, 1.5 and 12 mol%) are presented in Fig. 2(b). The observed reflections were (100), (002), (101), (102), (110), (103), (112) and (201). It has been observed that the XRD peak broadening increases with increase of doping concentrations. The XRD of undoped and Mn doped $ZnO_{(1-x)}S_x$ pattern reveals the formation of a product indexed to the hexagonal wurtzite phase of ZnS (JCPDS, card no. 36-1450). The intensity of these reflections slightly decreases with rise in doping. It is well known that the lattice parameters are Mn-doping dependent, i.e. an increase in Mn doping leads to contraction of the lattice as reported by Ali et al. [7]. The crystallite size was estimated from the Debye formula [8,9] using the XRD line broadening as follows:

$$B = \frac{k\lambda}{s\cos\theta} \tag{1}$$

where $s$ is the crystallite size, $\lambda$ is the wavelength of the X-ray radiation (CuKα=0.15406 nm), $k$ is a constant taken as 0.94, $\theta$ is the diffraction angle and $B$ is the line width at half maximum height. All major diffraction peaks for all samples are chosen to estimate the crystallite sizes using the least square fit method. It was found that the crystallite size of ZnOS nanopowder was around 19.9 nm for undoped ZnOS samples which decreased to 9.6 nm when the sample was doped with 12 mol% of Mn. The lattice parameters (a and c) and crystallite size as a function of dopant concentrations are shown in Table 1 and it was observed that there is a continuous decrease in the lattice parameter and particle size with Mn concentration. ZnOS alloys with a wurtzite structure were achieved for small content of sulfur and no evident phase separation was observed in the investigated composition range as determined by X-ray diffraction. Generally bulk wurtzite is metastable relative to the cubic phase below 1020 °C. Here, in sol–gel conditions, stable wurtzite ZnS nanostructures are formed at much lower temperatures (150–230 °C). The broad XRD peaks exhibit particles that are naono sizes.

**Table 1**
Variation of crystallite size and lattice parameters with amount of Mn content.

| | Undoped ZnOS | ZnOS: Mn 0.5 mol% | ZnOS: Mn 1.5 mol% | ZnOS: Mn 12 mol% |
|---|---|---|---|---|
| Size (nm) | 19.87 | 18.01 | 16.25 | 9.6 |
| $a$ (nm) | 3.2699 | 3.2676 | 3.2632 | 3.2262 |
| $c$ (nm) | 5.2323 | 5. 2309 | 5.2267 | 5.2001 |
| $c/a$ | 1.6 | 1.6 | 1.6 | 1.6 |

The effect of different Mn concentrations on the optical properties such as absorbance and band gap of $ZnO_{(1-x)}S_x$ nanoparticles were investigated. The absorbance of ZnOS nanoparticles was measured in the wavelength range from 200 to 700 nm. The UV–visible absorption spectra of undoped and Mn doped $ZnO_{(1-x)}S_x$ nanocrystals at different Mn dopant concentrations are shown in Fig. 3(a). All the samples showed absorption maximum of ZnS at 271 nm and high transmittance in UV and visible region, respectively. The optical absorption measurements show strong excitonic peak emission without any defect emission in the visible spectrum. No new absorption peak appears in the UV–visible spectra. It is clearly seen that $ZnO_{(1-x)}S_x$ is a typical direct gap semiconductor with no absorption in the visible light region. Clearly, the absorption edge is seen to shift to the higher wavelengths with Mn-dopant content in the precursor, indicating changes in particle sizes. The presence of the Mn dopant diminishes the excitonic emission. The decrease in absorbance could be attributed to the larger surface to volume ratio of $ZnO_{(1-x)}S_x$ nanoparticles which in turn increases its Rayleigh scattering [10]. The presence of the Mn dopant diminishes the excitonic emission. The absorption maximum of $ZnO_{(1-x)}S_x$ was plotted against the Mn concentration, as shown by square in Fig. 3(c). The % absorbance was observed to be lower in the case of 12 mol% Mn doping and increased with low doping concentrations. The band-gap energy ($E_g$) was estimated from absorption measurements using the Tauc formula [11] given by

$$\alpha = \left(h\nu - E_g\right)^n A/h\nu(h\nu)^2 \sim (h\nu - E_g) \tag{2}$$

The graph of $(Kh\nu)^2$ versus $h\nu$ (Fig. 3(b)) is obtained in by extrapolating the graph to $x$-axis $(Kh\nu)^2=0$ to give a value of the optical energy gap of the samples.

The bandgap energies of the ZnOS nano-particles were calculated and found to change from 4.0 to 4.2 eV, which compares favorably with the literature value for hexagonal ZnS, measured at room temperature, of 3.7 eV. The values lie slightly above the band gap wavelength of 335 nm ($E_g$=3.7 eV) of bulk ZnS [12]. The band gap is observed to increase with an increase in Mn-doping concentrations, implying that the optical properties of these materials are affected by the dopant. It was noticed that the bandgap values were higher than the bulk value of ZnS (3.7 eV) due to quantum confinement in the $ZnO_{(1-x)}S_x$ nanocrystallites. By increasing the Mn content, the powders exhibited or decrease in both the $a$ and

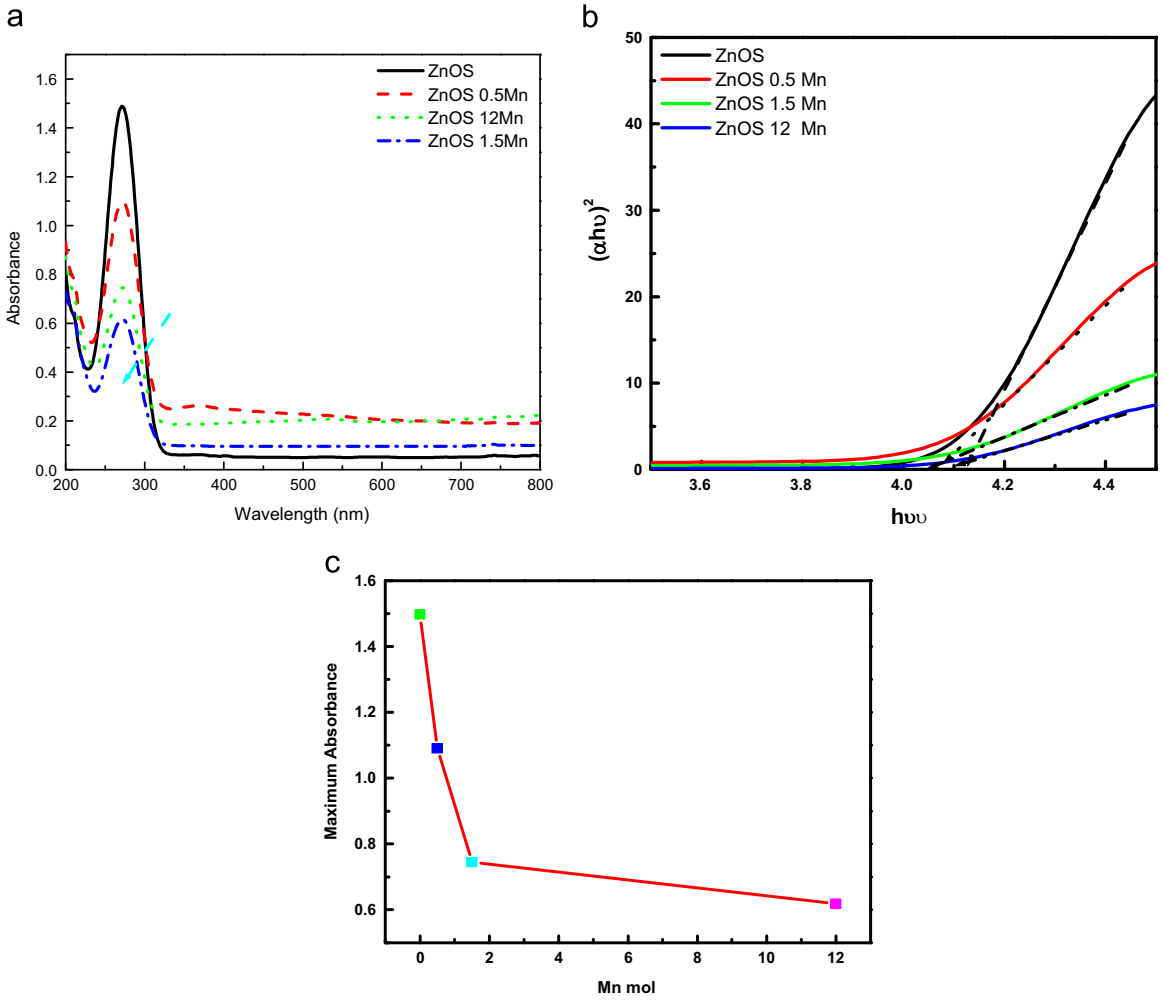


**Fig. 3.** (a) UV–vis absorption spectra and (b) determination of band gap of precipitation method synthesized $ZnO_{(1-x)}S_x$ nanoparticles from UV–vis measurements. The band gap of the material is calculated to be 4.12 eV, a value which is comparable to the literature value of 3.7 eV. (c) Variation of maximum absorbance undoped and Mn-doped $ZnO_{(1-x)}S_x$ nanoparticles as a function.of Mn-dopant concentrations.

*c*-axis lattice possibly due to the internal variable stress or defect in the lattice [13,14]. The compressed lattice is expected to provide a wide band gap because of the increased repulsion between the oxygen 2p and the zinc 4s bands.

The PL is used to further investigate the optical properties of the as synthesized $ZnO_{(1-x)}S_x$ nanopartciles. Owing to the large band gap of ZnS, it can readily host different transition metal ions as luminescent centers. It has been reported that the dopants of Cu, Mn or Cd can shift the luminescence position of ZnS nanocrystals [15–17]. Of these transition metal ion doped nanostructures, $Mn^{2+}$ ion doped ZnS is more important because of its optical as well as magnetic properties as a spintronics material. Thus, the synthesis of high-quality Mn-doped ZnS nanostructures is very important from the perspective of future spintronics research. Although detailed results of Mn-doped ZnS nanostructures have been published elsewhere [15,16], we would like to include a brief discussion of undoped and Mn-doped ZnS nanoparticles to show that the sol-gel synthesis approach is quite capable of addressing the high Mn concentration doping issue in semiconductor nanostructures without any major modification of the synthesis approach. The doped nanostructures were synthesized by introducing appropriate amounts of manganese acetate salt as the source of Mn, keeping the rest of the parameters unchanged. Fig. 4 shows the spectra of undoped and Mn-doped ZnS nanoparticles synthesized under identical conditions. It is well know that the pure ZnS nanoparticle [17–21], emit in the blue ($\lambda_{em}$=424–450 nm) upon UV excitation. The room temperature PL spectrum is

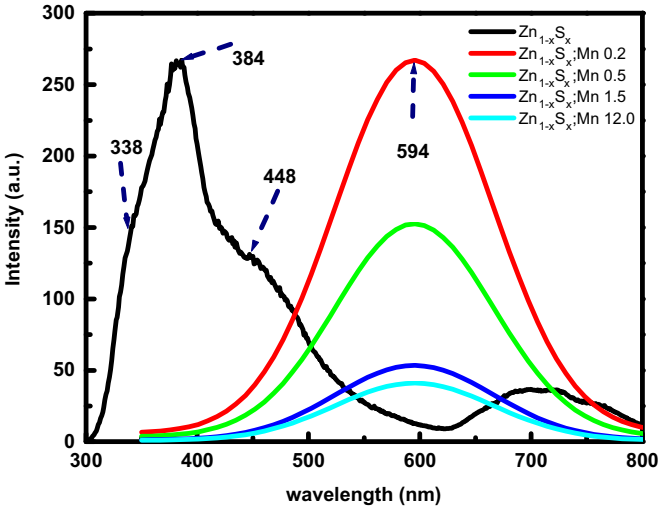


**Fig. 4.** PL spectra of undoped and Mn-doped $ZnO_{(1-x)}S_x$ nanoparticles at room temperature. The emission peaks of undoped $ZnO_{(1-x)}S_x$ indicate peak deconvolution by Gaussian fit. (For interpretation of the references to color in this figure legend, the reader is referred to the web version of this article.)

shown in Fig. 4. As shown in Fig. 4, peak deconvolution by Gaussian fit (not shown) for undoped ZnS spectra gives four bands centering at about 338 nm, 384 nm, 448 nm and 705 nm, respectively (the lower

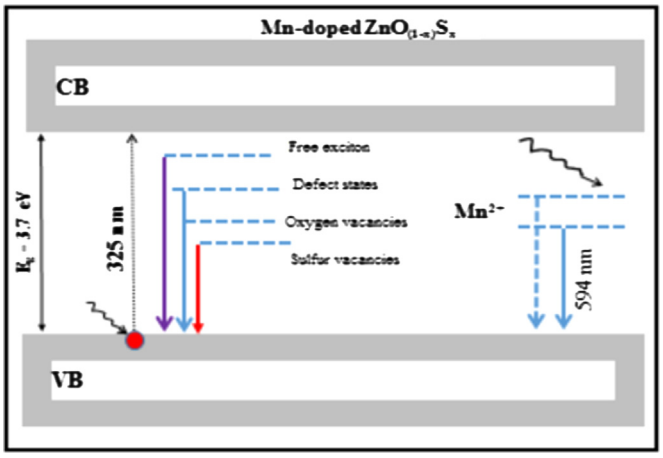


**Fig. 5.** Schematic energy level diagram for the mechanism of undoped and Mn-doped $ZnO_{(1-x)}S_x$ nanoparticles emissions at room temperature obtained from the PL spectra.

bands shown in Fig. 4). A similar result was also observed by other researchers [21,22]. PL emission peak at 338 nm (3.7 eV) corresponds to the bandgap energy of $ZnO_{(1-x)}S_x$ nanostructures. The emission peak at 384 nm could be assigned to free-exciton recombination. The blue emission at about 448 nm corresponds to the transition from the conduction band to the lower lying energy levels such sulfur vacancies [23]. This could also be assigned to the impurities or defect centers in the ZnS nanoparticles, which has been reported by some literature [18]. The low and high concentration of S and oxygen ions in $ZnO_{(1-x)}S_x$, respectively which was given by EDS as shown in Fig. 2 (a) causes large number of sulfur vacancies and oxygen interstitials that can act as doubly ionized donor centers. The corresponding schematic energy level diagram is shown in Fig. 5. The ZnS nanoparticles doped with Mn ions exhibit strong orange emission at $\approx$ 594 nm. The PL spectra of the Mn-doped samples exhibit a strong orange emission attributed to the $^4T_1$–$^6A_1$ transition of the $Mn^{2+}$ ions. The exhibition of an almost defect-free $Mn^{2+}$ ionic transition related orange emission from the Mn-doped ZnS nanostructures indicated that high-quality doped nanostructures could be synthesized following a similar synthetic approach to those of their undoped counterparts. While it is known that the $Mn^{2+}$ doped ZnS nanoparticles have two emission bands. One is blue ($\lambda_{em}$=400 nm) which is attributed to the self-activated emission caused by Zn vacancies in the lattice, another is orange–yellow ($\lambda_{em}$=585 nm) emission. Our samples have shown only a single yellow emission. As $Mn^{2+}$ ions on $Zn^{2+}$ sizes, where the $Mn^{2+}$ is tetrahedrally coordinated by sulfur [19], the $Mn^{2+}$ ions excited via energy transformation of the $ZnO_{(1-x)}S_x$ host efficiently and produced the $^4T_1$–$^6A_1$ transition that result in the orange emission [18–21]. Similar to our findings they also pointed out that the orange emission does not seem to be influenced by the nanoparticle size, there is no size effect reported so far on the peak position of this radiative transition.

## 4. Conclusion

In summary, we have successfully synthesized zinc sulfide nanoparticles by using a simple precipitation method. SEM study indicated a smooth and dense surface morphology that changes from flake like to spherical particles with an increase in Mn-doping. The x-ray diffraction results show that the powders are polycrystalline in nature. The crystallite sizes of the nanoparticles were determined, and found to be in the range of 9.6–19.9 nm.The bandgap energies of the ZnOS nano-particles were calculated and found to change from 4.0 to 4.2 eV, which compares favorably with the literature value for hexagonal ZnS, measured at room temperature, of 3.7 eV.

## Acknowledgments

The authors send immense gratitude to the South Africa's National Research Foundation (NRF), the University of the Free State physics department and the Organization for the Prohibition of Chemical Weapons (OPCW) for the financial assistance for this study.

## References

[1] M.Y. Chen, C.C. Chang, Jpn. J. Appl. Phys. 48 (2009) 112201.
[2] M. Labrenz, G.K. Druschel, T. Thomsen-Ebert, B. Gilbert, S.A. Welch, K. M. Kemner, G.A. Logan, R.E. Summons, G.D. Stasio, P.L. Bond, B. Lai, S.D. Kelly, J. F. Banfield, Science 290 (2000) 1744.
[3] H. Pang, Y. Yuan, Y. Zhou, J. Lian, L. Cao, J. Zhang, X. Zhou, J. Lumin. 122 (2007) 587.
[4] A.P.J. Alivisatos, Phys. Chem. 100 (1996) 13226.
[5] G. Shen, J.H. Cho, S.J.K. Yoo, G.-C. Yi, C.J. Lee, J. Phys. Chem. B 109 (12) (2005) 5491–5496.
[6] B.K. Meyer, A. Polity, B. Farangis, Y. He, D. Hasselkamp, Th. Krämer, C. Wang, Appl. Phys. Lett., 85, (2004) 4929.
[7] A.G. Ali, F.B. Dejene, H.C. Swart, Central Eur. J. Phys. 10 (2) (2011) 478–484.
[8] L. Ying, L.S. Hon, T. White, R. Withers, L.B. Hai, Mater. Trans. 44 (2003) 1328–1332.
[9] M.A. Barakat, G. Hayes, S. Ismat Shah, J. Nanosci. Nanotechnol. 5 (2005) 1–7.
[10] C.F. Bohren, D.R. Huffman, Absorption and Scattering of Light by Small Particles, John Wiley & Sons Inc., Hoboken, NJ, 1983.
[11] J.I. Pankove, Optical Processes in Semiconductors, Prentice-Hall, Englewood Cliffs, NJ, 1971.
[12] Y. Zhu, Y. Bando, D. Xue, D. Golberg, J. Am. Chem. Soc. 125 (2003) 16196.
[13] Y.C. Lin, B.L. Wang, W.T. Yen, C.T. Ha, C. Peng, Thin Solid Films 518 (2010) 4928.
[14] R. Ghosh, D. Basak, S. Fujihara, J. Appl. Phys. 96 (2004) 2689.
[15] S. Biswas, S. Kar, S. Chaudhuri, J. Phys. Chem. B 109 (2005) 17526.
[16] S. Kar, S. Biswas, S. Chaudhuri, P.M.G. Nambissan, Nanotechnology 18 (2007) 225606.
[17] R.N. Bhargava, D. Gallagher, Phys. Rev. Lett. 72 (1994) 416.
[18] R.N. Bhargava, J. Lumin. 70 (1996) 85.
[19] A.A. Bol, A. Meijerink, Phys. Rev. B 58 (1998) R15997.
[20] K. Sooklal, B.S. Cullum, S.M. Angel, C.J. Murphy, J. Phys. Chem. 100 (1996) 4551.
[21] In: Z.L. Wang et al. (Ed.), Handbook of Nanophase and Nanostuctured Materials—Synthesis, Tsinghua University Press and Kluwer Academic/Plenum Publishers, 2002.
[22] Y. Jiang, X.M. Meng, J. Lui J, Z.Y. Xie, L.S. Lee, S.T. Lee, Adv. Mater. 15 (2003) 323.
[23] D. Kurbatov, V. Kosyak, A. Opanasyuk, V. Melnik, Physica B404 (2009) 5002.